Matrix element effects in angle-resolved valence band photoemission with polarized light from the Ni(111) surface

M. Mulazzi,[1,2,*] M. Hochstrasser,[3] M. Corso,[4] I. Vobornik,[1] J. Fujii,[1] J. Osterwalder,[4] J. Henk,[5] and G. Rossi[1,2]
[1]*Dipartimento di Fisica, Università degli Studi di Modena e Reggio Emilia, Via Campi 213/A I-41100 Modena, Italy*
[2]*TASC National Laboratory, InFM-CNR, S.S. 14, km 163.5, I-34012 Trieste, Italy*
[3]*Laboratorium für Festkörperphysik, Wolfgang-Pauli-Strasse 16, ETH Hönggerberg, CH-8093 Zürich, Switzerland*
[4]*Physik-Institut, Universität Zürich-Irchel, CH-8057 Zürich, Switzerland*
[5]*Max Planck Institute of Microstructure Physics, Theory Department, Weinberg 2, D-06120 Halle (Saale), Germany*
(Received 13 April 2006; revised manuscript received 19 June 2006; published 26 July 2006)

Photoemission intensities from angle-resolved photoelectron spectroscopy with polarized synchrotron radiation were measured and calculated for a magnetization averaged Ni(111) single-crystal surface. Concentrating on the large variations of intensity in dependence on the experimental geometry and parameters, we discuss the exchange-split *sp* bands crossing E_F and identify strong matrix-element effects that are not dependent on selection rules involving parity. Comparison of experimental intensities with *ab initio* photoemission calculations provides a firm basis for disentangling symmetry from intrinsic effects due to the initial state. The calculated spectra provide a direct connection between ground-state properties (given by the spectral function) and the experimental intensities.

DOI: 10.1103/PhysRevB.74.035118 PACS number(s): 79.60.−i, 71.20.−b, 73.20.At, 75.70.Rf

I. INTRODUCTION

Angle-resolved photoelectron spectroscopy (ARPES) is the only technique which is able to determine simultaneously in-plane momentum and kinetic energy of photoelectrons.[1] These two quantities are related—due to translational invariance and energy conservation—to the binding energy and the in-plane wave vector that the electron possessed *before* the excitation. The normal component of the wave vector is in principle not determined but by choosing suitable setups this problem can be overcome.[2,3] For this reason ARPES is commonly used to determine the dispersion $E(\vec{k})$ of electronic states in solids (so-called band mapping). But, a photoemission spectrum contains much more information than just the binding energy of the occupied electronic states. Up to now a complete description of the peak line shape has not been reached: approximations holding for the case of flat bands and moderate electronic correlations are obtained by the Lorentz distribution;[1] the energy dispersion for initial and final states do contribute to the peak shape due to the broadening of the k_{perp} conservation. The historical development of ARPES has been based on the capability of E vs $\vec{k}$ mapping of direct transitions, i.e., by selecting from the data the energy values of main peaks regardless of line shape, background, or absolute intensity. The role of the matrix elements which essentially determine the heights of the intensity maxima was only marginally considered, although this is the main ingredient determining the experimental intensity distribution, i.e., the photoemission signal.[4–12] Recently, however, peak widths were investigated in strongly correlated electron systems (e.g., cuprate superconductors and heavy fermion systems), since these are considerably influenced by the hole and electron lifetimes, the latter being directly connected to the excited state and ground-state correlations through the respective self-energies.[4,10] Following Ref. 1, we write the spectral function as

$$A(\vec{k},\omega) = -(1/\pi)\mathcal{I}G(\vec{k},\omega),$$

where $G(\vec{k},\omega)$ is the one-particle Green function.

It is defined as $G(\vec{k},\omega)=1/[\omega-\varepsilon_{\vec{k}}-\Sigma(\vec{k},\omega)]$, where $\Sigma(\vec{k},\omega)$ is the self-energy function. The simple poles of the Green function give the eigenvalues of the Hamiltonian of the interacting system. In the noninteracting case, the self-energy vanishes and the Green function reduces to a sum of δ functions giving the band structure in the one-electron approximation.

The self-energy function contains all the information about the many-particle interactions and their effect on the electronic structure. $\Sigma(\vec{k},\omega)$ is a complex function of the binding energy and electron momentum, $\Sigma(\vec{k},\omega)=\Sigma'(\vec{k},\omega)+i\Sigma''(\vec{k},\omega)$, both terms of which have an effect on the spectral function.

The explicit expression of the last quantity is

$$A(\vec{k},\omega) = -\frac{1}{\pi}\frac{1}{\Sigma''(\vec{k},\omega)}\frac{1}{1+\left(\dfrac{\omega-\varepsilon_{\vec{k}}-\Sigma'(\vec{k},\omega)}{\Sigma''(\vec{k},\omega)}\right)^2},$$

which tells that the general expression of the spectral function is a Lorentzian peak whose maximum lies at $\varepsilon_{\vec{k}}+\Sigma'(\vec{k},\omega)$ having a half-width of $\Sigma''(\vec{k},\omega)$ and height equal to $1/\Sigma''(\vec{k},\omega)$. Despite the simplicity of the formula, the behavior of the self-energy is very complicated and not known in general. However, it is possible to see that the real part of the self-energy changes the position of the peak, i.e., shifts the binding energy of the electron states, while the imaginary part of the self-energy increases the peak width and lowers the peak height.

There is clearly a great interest in better understanding the relation between photoemission intensities and spectral functions since much information on the electronic structure be-

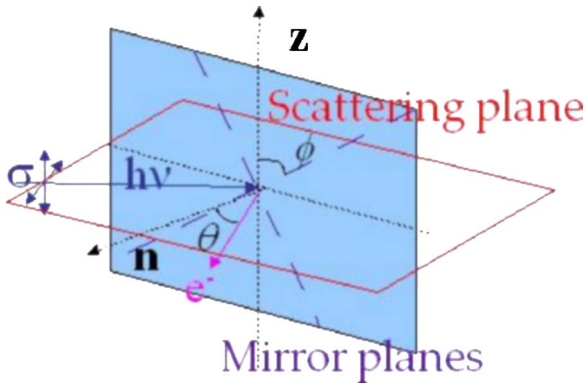

FIG. 1. (Color online) Experimental setup: σ indicates the polarization vector of the incident light that can be controlled by acting on the photon source; *s*, *p*, or left- and right-handed circular polarization. The scattering plane is spanned by the photon and photoelectron momenta, which are coplanar with the surface normal. Through the azimuthal degree of freedom ϕ the sample rotation about the surface normal is performed, while the rotation about the *z* axis changes the polar angle θ of detection. Analyzer axis and the photon beam are fixed in space at an angle of 43° in the scattering plane, i.e., normal emission spectra are obtained at an oblique light incidence angle of 43°.

yond E vs $\vec{k}$, including band degeneracy and correlations, would become retrievable from photoemission data sets measured controlling (possibly all) the experimental parameters. This situation is, however, seldom realized because the photoemission intensity strongly depends on matrix elements.

Basically being an overlap integral between an initial-state wave function $\psi_i(\vec{r})$ transformed according to the interaction operator H_{int} (e.g., dipole operator $H_{\text{int}}=\hat{e}\cdot\vec{p}$, where $\hat{e}$ indicates the polarization unit vector and $\vec{p}$ the electron momentum operator) and a final-state wave function $\psi_f(\vec{r})$, these depend on the photoelectron momentum and modulate the intensities according to the parameters used in the experimental setup (such as photon incidence angle, energy and polarization, electron emission angle, and kinetic energy),

$$\langle\psi_f|H_{\text{int}}|\psi_i\rangle = \int \psi_f^*(\vec{r})H_{\text{int}}\psi_i(\vec{r})d^3r = \int \psi_f^*(\vec{r})(\vec{e}\cdot\vec{p})\psi_i(\vec{r})d^3r.$$

However, there are situations in which matrix element effects can be exploited to gain information on the initial state from the experimental photoemission spectra. In particular configurations, e.g., if photon momentum, photoelectron momentum, and surface normal lie in a mirror plane of the crystal (cf. Fig. 1 for the particular case of $\phi=0°$), a matrix element can be strictly zero, depending on the polarization of the incident light and the symmetry of the initial-state wave function.[13]

Because the final state is even with respect to a mirror operation far away from the sample (i.e., at the detector), it is even also in the crystal.[13] The parity of the dipole operator is completely determined by the polarization vector: it is even for *p* polarization and odd for *s* polarization. The initial-state wave function has a well-defined parity, too. In order to be nonzero the product of the terms intervening in a matrix element must be even under reflection. Since the final state is even, both the interaction operator and the initial state have to be simultaneously even or odd. In the first case (even), an experiment with *p* polarization detects only the even components of the initial-state wave function, while in the second case (odd) the odd components are measured with *s* polarization. State of the art electron analyzers capable of two-dimensional (2D) parallel detection and synchrotron radiation beamlines with variable phase undulator sources allow polarization-dependent photoemission experiments to be carried out. Large changes of the peak intensities are measured upon change of the light polarization, even in nonsymmetric configurations.[12,14–17] The photoelectron intensities measured off mirror planes cannot be interpreted on the basis of the symmetry selection rules; it is necessary to compare them to photoemission calculations in order to obtain information on the initial electron states.

Besides the selection rules that appear due to the crystal symmetry (these are considered in the present work), there are "atomic" selection rules that do not rely on the crystal ($\Delta L=\pm1$, $\Delta m=\pm1$ or $\Delta m=0$, depending on the polarization of the light[1]). The former can be exploited by using different light polarizations, resulting in "switching on or off" of the excitation of initial states with well-defined parity. In contrast, the latter can be regarded as intrinsic since they determine the actual peak height. They depend on the light polarization too because the dipole operator enters the expression of the atomic matrix elements explicitly. For complex intensity patterns (spectra), the problem of how to disentangle both types of selection rules arises. In this work, we follow a twofold approach: (a) detailed experiments using various symmetric and nonsymmetric setups, different photon energies, and polarizations and (b) first-principles photoemission calculations. The latter provide a direct link between the experimental intensities and the theoretical spectral function.

We concentrate the discussion on the photoemission intensities of the exchange-split *sp* states of Ni(111), at room temperature. The spin polarization of the *sp* exchange split states was probed earlier by spin-resolved experiments by Hoesch *et al.*[18] We measured two sets of photoemission intensities from the *sp* bands with both linear (*p* and *s*) and circular (left- and right-handed) polarizations in a ±15° azimuth angular range and in a ~1 eV binding energy range below the Fermi level using two photon energies ($h\nu$ =21.5 eV and $h\nu$=30 eV). The *sp* bands are observed to cross the Fermi level in the stereographic representation of the Fermi surface map. The three regions of the map showing the *sp* states are labeled *R*1, *R*2, and *R*3 in Fig. 2 and lie about the mirror planes of the (111) surface.

The differences between the experimental spectra taken in different conditions are attributed to strong matrix element effects that are reproduced by *ab initio* photoemission calculations. The agreement between the experimental and the theoretical data allows one to identify the effects of atomic matrix elements and to disentangle them from the symmetry-related contributions of the initial states. Thus, photoemission calculations prove to be necessary for the interpretation of, in general, complicated photoelectron intensity patterns.

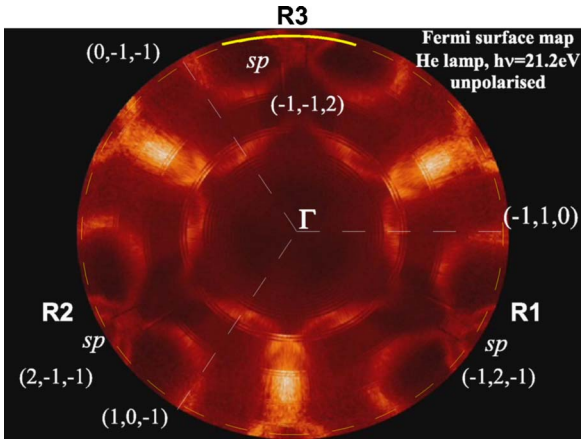

FIG. 2. (Color online) Stereographic representation of the Fermi surface map of the Ni(111) single crystal as being measured with unpolarized radiation from a He discharge lamp ($h\nu$=21.22 eV) at 300 K in the remanence state (demagnetized). The complete angular data set is divided into three equivalent sectors reflecting the threefold rotational symmetry of the (111) surface. $R1$, $R2$, and $R3$ indicate the *sp* states that cross the Fermi level, displaying exchange splitting. By tracing the photoemission intensity along one circle of the map one obtains the momentum distribution curve (MDC) of photoelectrons originating from the Fermi level, at the corresponding polar angle (from 0 to 79° off normal emission). The yellow solid line indicates the polar angle (θ=78°) at which the azimuthal MDCs, reported in Fig. 4, have been measured, while the yellow dashed line represents the k points at which the data of Fig. 3 have been measured and those of Fig. 5 have been calculated.

II. EXPERIMENTAL DETAILS

All data were collected at the low-energy branch of the APE beamline (INFM) installed at the Elettra synchrotron. We exploited all the possible polarizations of the Apple II nonperiodical undulator available in the whole photon energy range (10–130 eV): horizontal (*p*-type) and vertical (*s*-type) linear as well as left and right circular. The Scienta SES-2002 electron spectrometer allowed the simultaneous detection in a 14° angular window, with a 0.3° angular resolution. The overall energy resolution is 6 meV, as measured at 15 K, while the data presented in this work were taken at 300 K.

Clean Ni(111) surfaces were routinely obtained by Ar^+ ion sputtering at 1 keV, followed by oxidizing in 10^{-7} mbar O_2 pressure and then annealing to 1000 K. After two such cycles the surface shows clear low-energy electron diffraction (LEED) patterns and in ultraviolet photoemission spectroscopy (UPS) spectra there is no sign of contaminant after the preparation.

The sample is cylindrical with a carved slot (picture frame).[18] The surface cleaning procedure required annealing at 1000 K and, following cooling down to room temperature (RT), the crossing of T_{Curie} was performed in a measured residual magnetic field of ~5 mG. This produced a domain pattern averaging to zero net magnetization, so the sample can be considered demagnetized. The data acquisition procedure consisted of measuring the photoemission spectra at different azimuthal angles in the "rotating crystal" setup. This means that the beam direction and the analyzer were fixed in space, while the sample was rotated about the surface normal (the azimuthal degree of freedom). With respect to moving or cylindrical mirror analyzers our setup has the advantage of keeping the polarization projections on the scattering plane constant as a function of the azimuths.

III. THEORETICAL DETAILS

Electronic-structure calculations were performed within the framework of the local spin-density approximation (LSDA) to density-functional theory (DFT), using Korringa-Kohn-Rostoker (KKR) methods.

In a first step, the electronic structure of the Ni(111) surface was determined self-consistently, allowing the muffin-tin potentials of the first seven Ni layers and of three adjacent vacuum layers to differ from the bulk potentials. Surface boundary conditions (i.e., semi-infinite Ni crystal and semi-infinite vacuum) were imposed, in contrast to a slab geometry. The obtained overall exchange splitting is about 0.6 eV, whereas the local magnetic moment is about $0.64\mu_B$ (in a bulk layer).

In a second step, photoemission spectra were computed in the one-step model using the self-consistent potentials as input. As is well-known, the theoretical description of Ni within the LSDA results in two major shortcomings. While the first one, the missing of the 6 eV satellite, is not important in the present investigation, the second is more serious. The exchange splitting in the LSDA calculations is about 0.6 eV while in experiment it is found to be about 0.3 eV. Further, the exchange splitting depends on the wave vector,[19,20] also not reproduced accurately by the LSDA. The origin for this disagreement is the strong electron correlation in Ni, which can be treated successfully when going beyond the LSDA.[21–23] In the present investigation, we chose to scale the difference of the spin-dependent LSDA potentials in order to reproduce the overall exchange splitting of 0.3 eV. This method leads to an approximate rigid shift of the bands but does not improve the wave-vector dependence of the splitting. Consequently, both the dispersion and the orbital character (and hence, the photoemission intensity) of some of the electronic states can differ from their experimental counterparts (see Sec. IV). In favor of the present approach we note that it was applied successfully for dichroic photoemission from Ni/Cu(001).[24] Free parameters in the photoemission calculations, such as lifetimes of initial and final states, were taken from earlier work.[25] Hence, within this approach all parameters in the calculations are fixed.

The intensities were computed within the spin-polarized relativistic layer-KKR method, thus treating spin-orbit coupling and magnetism on equal footing. By this means, the orientation of the magnetization is fully accounted for, thus allowing investigation of magnetic dichroism.

IV. RESULTS

The data presented in Figs. 3(a) and 3(b) show four main features, each behaving differently upon a change of light polarization. They are the *sp* bands (A), the minority *d* band

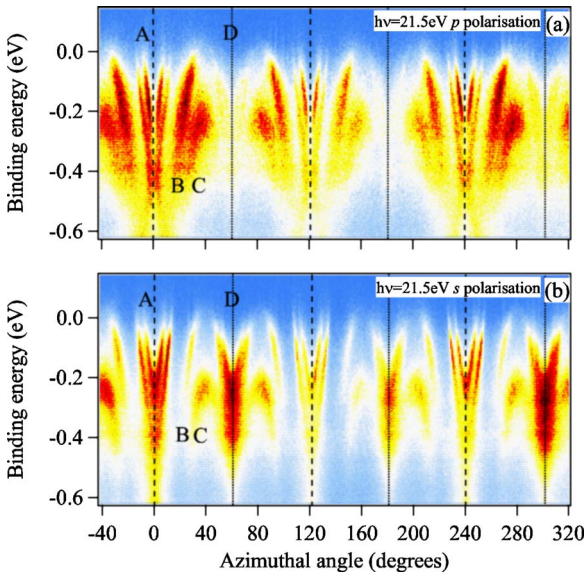

FIG. 3. (Color online) Two 360° photoemission maps measured with $h\nu$=21.5 eV at 78° off-normal emission (see the yellow dashed line of Fig. 2) with (a) p and (b) s polarization. The azimuthal step size is 1° and the polar angle is integrated over $\Delta\theta$ =1°. The letters mark angles at which bands show up that are discussed in the text. Because of the threefold symmetry of the demagnetized state, the images are made up of three equivalent regions, each of which contains two distinct mirror planes highlighted by the vertical dashed and dotted lines. Extracting the photoemission intensities along a vertical line, one obtains an energy distribution curve (EDC) at a given azimuthal angle. Similarly, plotting the data along a horizontal line, one obtains the MDC at the corresponding initial state energy with respect to the Fermi level. Summing data sets (a) and (b) and extracting a MDC at E_F (E_B=0 eV), one retrieves the same information as contained in the data of Fig. 2 along a circle located at θ=78° from normal emission (apart from the small difference of the photon energy used in the two measurements).

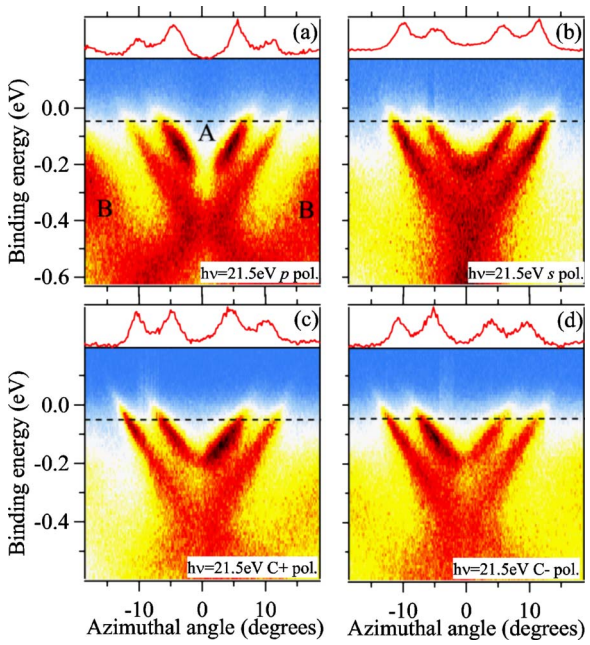

FIG. 4. (Color online) ARPES angular maps of the sp states within ~0.6 eV range of binding energy below the Fermi level are collected at $h\nu$=21.5 eV using a $\Delta\phi$=0.2° step with (a) p; (b) s; (c) right-handed circular and (d) left-handed circular polarizations. In the top part of each image a MDC taken at E_B=50 meV is shown and the k points at which the insets were extracted are highlighted by a black dashed line. The letters "A" and "B" in (a) identify the sp states and the minority d bands according to the definition given for Fig. 3 (these labels are omitted in the other images).

(B), the majority d band (C), and the group of states (D), which is found probably due to a second photoemission cone.[26] The relative intensities change dramatically if the linear polarization is turned from p to s, while the binding energies of the features remain constant (within an experimental error of ~20 meV). This means that the experiment probes all bands regardless of the light polarization, but the intensity distribution, on the contrary, depends severely on it. This effect is termed linear dichroism in the angular distribution (LDAD) of photoelectrons and was intensively studied for photoemission from core levels,[27–33] whereas for valence band ARPES significantly less work was performed.[12]

All the sp states [feature A in Fig. 3, also highlighted in Figs. 4(a) and 4(b)] undergo very strong intensity variations when rotating the light polarization. The intensity close to the symmetry axis between the sp bands, at ϕ=0° in Fig. 4, drastically increases when the polarization turns from p to s; the symmetry selection rules apply and we infer that at a mirror plane the initial states are odd. Moving away from the symmetric configuration, the mirror symmetry is lost and the symmetry selection rules are no longer valid; the parity of the initial state is not well-defined. Features B and C also show large variations upon polarization rotation. For p-polarized light B is the most intense feature, while for s-polarized light its intensity is strongly reduced. Also the intensity of feature C measured with s polarization is lower than that obtained with p polarization, but this change is less strong than for feature B.

Feature D, lying at a mirror plane, shows the largest intensity change when the light polarization is turned by 90°. While it is faintly visible with p-polarized light, it shows up as intense as feature A with s polarization. Hence, also feature D is odd upon reflection at a mirror plane.

Altogether, the data of Fig. 3 show that the photoemission intensity, in a given experimental geometry, depends strongly on the light polarization throughout the whole Brillouin zone. These large changes call for a theoretical analysis by means of first-principles photoemission calculations in order to provide more information, thus going beyond parity considerations.

The theoretical ARPES angular maps (Fig. 5) were calculated considering all experimental parameters used to gather the data of Fig. 3. The calculated dispersion relations agree reasonably well with the experimental ones, as shown in the momentum distribution curves (MDCs) of Fig. 6 taken at E_B=70 meV, thus supporting the scaling approach for the self-consistent potentials. All experimental features are correctly reproduced and show up three times, as expected for the threefold rotational symmetry of the (111) surface. Also, the intensity patterns, and in particular the intensity redistri-

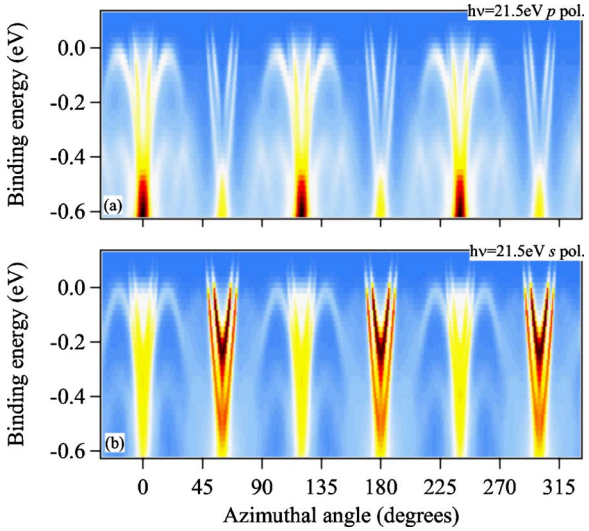

FIG. 5. (Color online) Calculated ARPES angular maps for (a) p polarization and (b) s polarization taking into account the parameters used to collect the data of Fig. 3 (the dashed yellow line of Fig. 2 shows the k points at which the calculation has been carried out). The images have been multiplied by the Fermi-Dirac distribution function with $k_BT=25$ meV for a best comparison with the experimental data.

bution induced by the polarization change, are in agreement with the experiment.

Figures 4(c) and 4(d) show the sensitivity of the ARPES maps to the excitation by circularly polarized light. As for linear polarized light, the band dispersions are symmetric with respect to a mirror plane, as expected, while the photoemission intensities are not. The intensity asymmetry is reversed when the helicity is reversed. These effects are understood by considering the parities of the initial states and of the polarization vector. The presented data were acquired in such a way that the photon momentum lies in the scattering plane, but only at azimuth $\phi=0°$, which coincides with a mirror plane. Because of this, the binding energies of the right side of the image are the same of those of the left. Let us consider the linear polarization vectors at two symmetric positions about the mirror plane, i.e., at generic angles ϕ and $-\phi$. The projections on the mirror plane of the two vectors coincide, while the projections on the axis perpendicular to

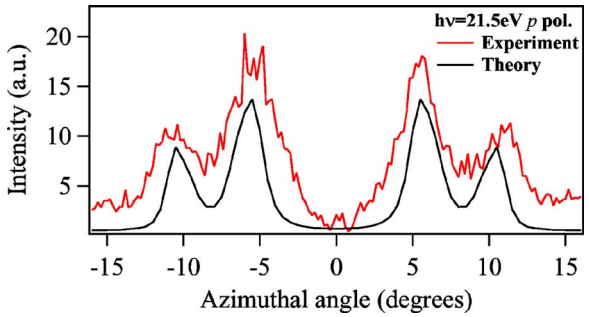

FIG. 6. (Color online) Comparison between the experimental (red line) and theoretical (black line) MDCs for the sp states as measured and calculated for p polarization at a binding energy of 70 meV. The width of the energy integration interval is 10 meV.

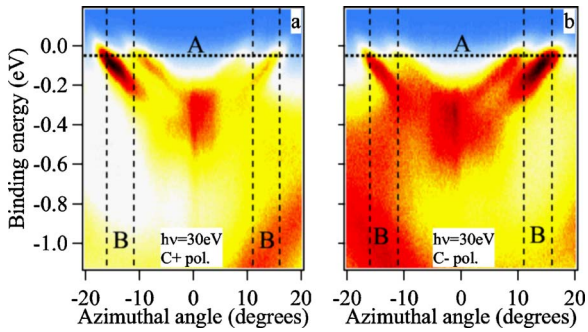

FIG. 7. (Color online) ARPES angular maps restricted to the sp states collected at $h\nu=30$ eV using $\Delta\phi=0.2°$ step size with (a) right-handed circular and (b) left-handed circular polarizations. The vertical dashed lines indicate the angles at which the EDCs of Fig. 8 are retrieved.

the mirror plane are equal in magnitude, but of opposite sign.[33] Since in the expression for the photocurrent the matrix elements show up squared, the sign of the projection does not matter. Thus, the intensities at symmetric positions with respect to the mirror plane have to be symmetric, for both p and s polarizations. Since in the actual experimental geometry the projections for the two types of polarizations are different, the intensity distributions of the sp states could differ. We readily observe the symmetry of the intensities with respect to the mirror plane on all the linear polarization data.

Things change when circularly polarized radiation is employed. Circular polarization is an axial vector, like magnetic field or angular momentum, that can be expressed as a complex combination of p and s polarizations: $\vec{C}+=\vec{s}+i\vec{p}$ or $\vec{C}$

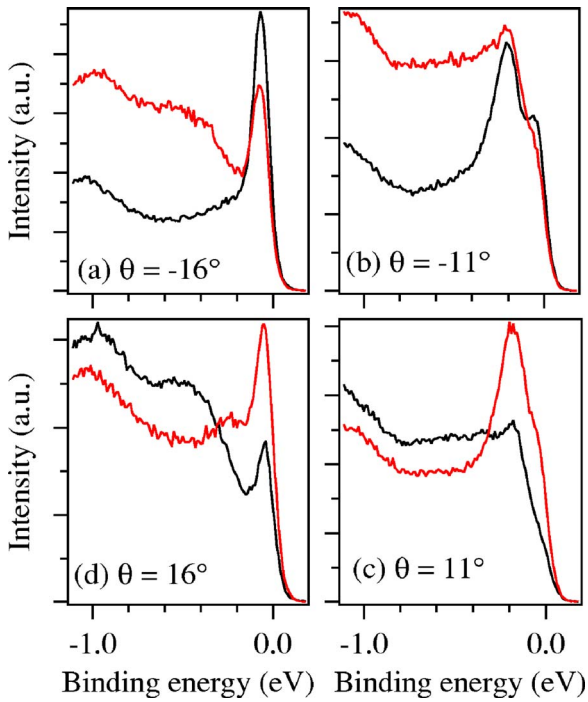

FIG. 8. (Color online) EDCs extracted from the ARPES maps of Fig. 7 at (a) $\theta=-16°$; (b) $\theta=-11°$; (c) $\theta=11°$; (d) $\theta=16°$ for (red line) left-handed and (black line) right-handed circular polarization.

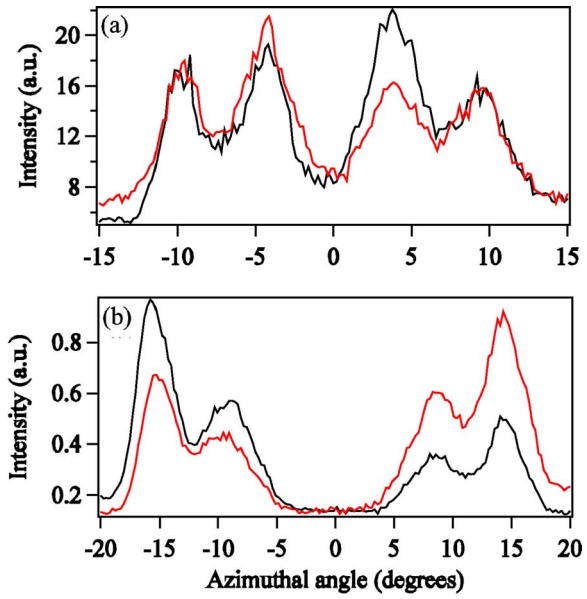

FIG. 9. (Color online) Experimental MDCs extracted from the ARPES angular maps measured with right (black line) and left (red line) circular polarization. The data in (a) are extracted at E_B =120 meV while those of (b) are taken at E_B=50 meV. The binding energy chosen for the two images is different to stress the effect of the circular light on the spectra. As explained in the text, the intensities at one side of the mirror plane with one polarization are very close to those measured on the opposite side of the mirror plane with the other circular polarization.

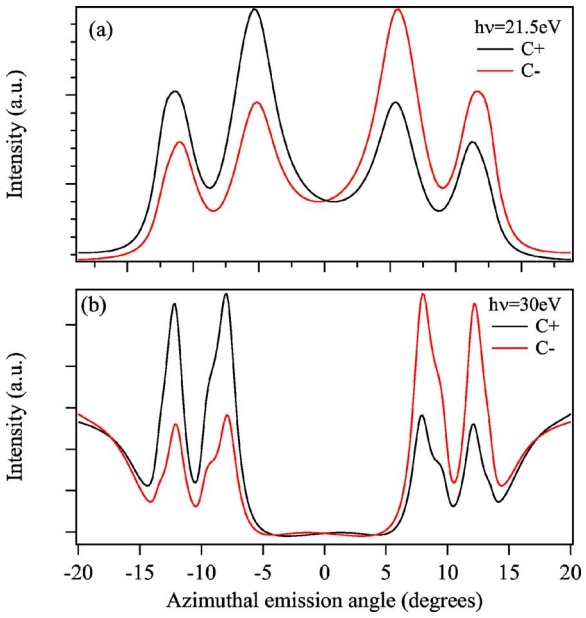

FIG. 10. (Color online) MDCs calculated, for comparison with Fig. 9, at (a) E_B=120 meV and (b) E_B=50 meV with the same parameters used in the experiments: angle of incidence of 43°, polar emission angle of 55°, right-handed (black line) and left-handed (red line) circular polarization, and a photon energy of (a) $h\nu$ =21.5 eV and (b) $h\nu$=30 eV.

$-=\vec{s}-i\vec{p}$. Reflection at the mirror plane reverses the *phase* of the polarization and, hence, $\vec{C}+\rightarrow\vec{C}-$ and $\vec{C}-\rightarrow\vec{C}+$. This in conjunction with the mirror symmetry implies for the intensities $I(C+,\phi)=I(C-,-\phi)$. Evidently, the mirror symmetry observed for linear polarization is lost [Figs. 4(c) and 4(d) obtained with $h\nu$=21.5 eV and Fig. 7 obtained with $h\nu$ =30 eV]. The energy distribution curves (EDCs) extracted from the data set of Fig. 7 and reported in Fig. 8 show in a more conventional representation the role of the symmetry on the circular polarization data. In these figures, as well as in Fig. 8, the data taken with one polarization at a given azimuth are very similar to those measured with the opposite polarization and at the respective negative azimuth. To show the importance of matrix elements' effects intervening upon circular polarization phase inversion, we did not normalize the curves to a common value.

The above considerations do not take into account the photon energy explicitly; thus, they are applicable to the data sets taken at both $h\nu$=21.5 eV and $h\nu$=30 eV. However, other relevant changes of the intensities appear to depend on the photon energy. At $h\nu$=21.5 eV, Fig. 4, and $h\nu$=30 eV, Fig. 7, the *d* bands (labeled *B* as in Fig. 3) at high binding energies and at $\phi\sim\pm18°$ lie on the same side of the image for the same polarization. On the contrary, the intensity of the *sp* states shifts from right to left (left to right) with right (left) circular polarization when increasing the photon energy. The *sp* states were previously identified, first by comparison with electronic-structure calculations, later by spin-resolved ARPES, as spin-split states with the majority band at a higher binding energy and, therefore, larger Fermi momentum (i.e., larger azimuth). Photoemission from the *sp* states at 21.5 eV shows the highest intensity for the minority states, while at 30 eV the largest intensity is for the majority states. The observed *sp* states are due to bulk bands, with full dispersion along *k* perpendicular as well as along *k* parallel to the surface. This is reflected in Figs. 4 and 7 in which the Fermi level crossings as measured at $h\nu$=21.5 eV take place at different azimuthal angles with respect to those measured with $h\nu$=30 eV. Changing the kinetic energy implies a change of the final states, leading consequently to different intensities originating from the same initial states.

Figure 9 reports four experimental momentum distribution curves (MDCs) for left and right circular polarization at $h\nu$=21.5 and 30 eV, respectively. The largest effect observed is a shift of the spectral weight from the left to the right of the symmetry plane for each dataset at the same photon energy. The theoretical calculations corresponding to these data are reported in Fig. 10 and are in good qualitative agreement with the experiment. Considering just Fig. 10(b) (corresponding to $h\nu$=30 eV), the theoretical peak positions calculated for E_B=50 meV are also in good agreement: $I_{\text{th}}^{\uparrow}=\pm12.15°$ and $I_{\text{th}}^{\downarrow}=\pm7.95°$, and $I_{\text{exp}}^{\uparrow}=\pm15.53°$ and $I_{\text{exp}}^{\downarrow}=\pm9.32°$, however, indicating a dispersion slightly too strong in theory [this feature was already found for the *L*-gap surface state of Au (111), corroborating an explanation by a too steep image-potential barrier[34]]. The theoretical peak widths, not convoluted with the instrumental resolution function and somewhat smaller than the experimental ones, are also in close agreement with the experimental data, supporting our choice of lifetime broadening.

The most important difference, however, lies in the peak height ratios: it is ~1 for the theoretical peaks lying on each

side of the mirror plane (beside the absolute intensity is different for those lying on opposite sides of the mirror plane), while the experimental minority-spin peaks are $\sim 1/2$ as intense as the majority-spin peaks lying on the same side of the mirror plane. Further tests in order to improve the free parameters in theory could not resolve this issue. Hence, we are led to conclude that the intensity differences might be attributed to deficiencies of the LSDA approximation used in the electronic-structure part of the calculations. On the other hand, we would like to note that the observed polarization dependence is well reproduced by the calculation.

The calculated photoemission intensities at 21.5 eV for circular polarization also show the spectral weight shifting from the left to the right upon polarization phase inversion. For this photon energy the agreement between the experimental and theoretical peak positions and the heights is quite good. Despite this agreement, the calculations do not describe the experimental shift of spectral weight from the left to the right of the mirror plane occurring when changing the photon energy from 21.5 to 30 eV. Theoretically, at both photon energies the most spectral weight for the same circular polarization lies on the same side of the mirror plane [cf. Figs. 10(a) and 10(b)]. In order to understand this disagreement we carried out calculations at photon energies close to the experimental ones (20, 23, 28, and 32 eV) in order to test the description of the final state. However, a shift of intensity from left to right or vice versa was not found. Since other spectral features are well described, a possible explanation could again be the inadequacy of the LSDA.

V. CONCLUSIONS

We addressed the interpretation of the large relative intensity changes of different bands measured in ARPES as a function of light polarization and energy by means of a detailed study of the spin-split *sp* bands of Ni(111) at room temperature. The experimental intensity patterns point to a large variation of the matrix elements in the photoemission process that are overimposed to other band structure effects. In order to disentangle symmetry versus atomic matrix element effects, a detailed description of the experimental geometry must be input for photoemission calculations from first-principles electronic structure. The direct comparison of theoretical and experimental data thus becomes possible and meaningful. We can therefore make statements on the matrix element effects, as well as appreciate the limits of the theory underlying the calculations for those experimental features that are not reproduced. The general agreement between experiment and theory warrants the identification of which of the three terms entering a matrix element (i.e., initial state, final state, and dipole operator) plays the most important role in the photoemission process, on the way to establishing a one-to-one relationship between spectral function and photoemission intensities.

The adopted *ab initio* approach for photoemission has produced good results for other materials, but not all the experimental information presented here; in particular, the $h\nu$ dependence of the photoemission intensities from Ni(111) is not well matched by the calculation. LSDA is not well adapted to describe electron correlations that are, on the other hand, very important for the good description of the electronic structure of nickel. It is certainly desirable that photoemission calculations proceed beyond the LSDA approximation, for example, by including the spin-dependent self-energy from dynamical mean-field theory (DMFT). The possibility of collecting a very rich set of intensities in the band mapping, and band tomography (i.e., kinetic energy dependent) mode at third-generation beamlines with energy and phase tunable photon sources, calls for a renewed effort in theory in order to make a step forward in the fine analysis of the electronic structure of solids and surfaces.

*Electronic address: mattia@issp.u-tokyo.ac.jp

[1] S. Hüfner, *Photoemission from Solids* (Springer-Verlag, Berlin, 1995), and references therein.
[2] P. D. Loly and J. B. Pendry, J. Phys. C **16**, 423 (1983).
[3] V. N. Strocov, R. Claessen, G. Nicolay, S. Hüfner, A. Kimura, A. Harasawa, S. Shin, A. Kakizaki, H. I. Starnberg, P. O. Nilsson, and P. Blaha, Phys. Rev. B **63**, 205108 (2001).
[4] N. V. Smith, P. Thiry, and Y. Petroff, Phys. Rev. B **47**, 15476 (1993).
[5] A. Gerlach, R. Matzdorf, and A. Goldmann, Phys. Rev. B **58**, 10969 (1998).
[6] M. B. Nielsen, Z. Li, S. Lizzit, A. Goldoni, and P. Hofmann, J. Phys.: Condens. Matter **15**, 6919 (2003).
[7] J. Henk, W. Schattke, H. Carstensen, R. Manzke, and M. Skibowski, Phys. Rev. B **47**, 2251 (1993).
[8] E. D. Hansen, T. Miller, and T.-C. Chiang, Phys. Rev. B **55**, 1871 (1997).
[9] X. Gao, A. N. Koveshnikov, R. H. Madjoe, R. L. Stockbauer, and R. L. Kurtz, Phys. Rev. Lett. **90**, 037603 (2003).
[10] A. Bansil, M. Lindroos, S. Sahrakorpi, and R. S. Markiewicz, New J. Phys. **7**, 140 (2005).
[11] S. V. Borisenko, A. A. Kordyuk, S. Legner, C. Dürr, M. Knupfer, M. S. Golden, J. Fink, K. Nenkov, D. Eckert, G. Yang, S. Abell, H. Berger, L. Forro, B. Liang, A. Maljuk, C. T. Lin, and B. Keimer, Phys. Rev. B **64**, 094513 (2001).
[12] T. Matsushita, S. Imada, H. Daimon, T. Okuda, K. Yamaguchi, H. Miyagi, and S. Suga, Phys. Rev. B **56**, 7687 (1997).
[13] J. Hermanson, Solid State Commun. **22**, 9 (1977).
[14] J. Schäfer, M. Hoinkis, E. Rotenberg, P. Blaha, and R. Claessen, Phys. Rev. B **72**, 155115 (2005).
[15] E. Rotenberg, W. Theis, K. Horn, and P. Gille, Nature (London) **406**, 602 (2000).
[16] R. L. Dubs, S. N. Dixit, and V. McKoy, Phys. Rev. Lett. **54**, 1249 (1985).
[17] D. Venus, Phys. Rev. B **48**, 6144 (1993).
[18] M. Hoesch, T. Greber, V. N. Petrov, M. Muntwiler, M. Hengsberger, W. Auwarter, and J. Osterwalder, J. Electron Spectrosc. Relat. Phenom. **124**, 263 (2002).

[19] H. Gollisch and R. Feder, Solid State Commun. **76**, 237 (1990).
[20] K. P. Kämper, W. Schmitt, and G. Güntherodt, Phys. Rev. B **42**, 10696 (1990).
[21] F. Manghi, V. Bellini, J. Osterwalder, T. J. Kreutz, P. Aebi, and C. Arcangeli, Phys. Rev. B **59**, R10409 (1999).
[22] F. Manghi, V. Bellini, and C. Arcangeli, Phys. Rev. B **56**, 7149 (1997).
[23] A. I. Lichtenstein, M. I. Katsnelson, and G. Kotliar, Phys. Rev. Lett. **87**, 067205 (2001).
[24] W. Kuch, A. Dittschar, K. Meinel, M. Zharnikov, C. M. Schneider, J. Kirschner, J. Henk, and R. Feder, Phys. Rev. B **53**, 11621 (1996).
[25] J. Henk and B. Johansson, J. Electron Spectrosc. Relat. Phenom. **94**, 259 (1998).
[26] G. Mahan, Phys. Rev. B **2**, 4334 (1976).
[27] Ch. Roth, F. U. Hillebrecht, H. B. Rose, and E. Kisker, Phys. Rev. Lett. **70**, 3479 (1993).
[28] M. Sacchi, G. Panaccione, J. Vogel, A. Mirone, and G. vander-Laan, Phys. Rev. B **58**, 3750 (1998).
[29] H. Ebert, L. Baumgarten, C. M. Schneider, and J. Kirschner, Phys. Rev. B **44**, 4406 (1991).
[30] C. Carbone and E. Kisker, Solid State Commun. **65**, 1107 (1988).
[31] F. Sirotti, G. Panaccione, and G. Rossi, Phys. Rev. B **52**, R17063 (1995).
[32] Ch. Roth, F. U. Hillebrecht, W. G. Park, H. B. Rose, and E. Kisker, Phys. Rev. Lett. **73**, 1963 (1994).
[33] J. Henk, T. Scheunemann, S. V. Halilov, and R. Feder, J. Phys.: Condens. Matter **8**, 47 (1996).
[34] J. Henk, M. Hoesch, J. Osterwalder, A. Ernst, and P. Bruno, J. Phys.: Condens. Matter **16**, 7581 (2004).